Dental pulp stem cell-derived extracellular vesicles loaded with hydrogels promote osteogenesis in rats with alveolar bone defects

XIN HE[1*], XIAO-YANG CHU[2*], XU CHEN[1], YU-LAN XIANG[1], ZE-LU LI[1], CHUN-YAN GAO[1], YING-YI LUAN[3], KAI YANG[3] and DONG-LIANG ZHANG[1]

[1]Department of Orthodontics, School of Stomatology, Beijing Stomatological Hospital, Capital Medical University, Beijing 100040, P.R. China; [2]Department of Stomatology, Fifth Medical Center of Chinese People's Liberation Army General Hospital, Beijing 100000, P.R. China; [3]Prenatal Diagnosis Center, Beijing Obstetrics and Gynecology Hospital, Capital Medical University, Beijing 100040, P.R. China

Received June 7, 2024; Accepted September 30, 2024

DOI: 10.3892/mmr.2024.13393

Abstract. Alveolar bone defects caused by inflammation, trauma and tumors adversely affect periodontal health, causing tooth loosening or dentition defects, thus affecting denture or implant repair. Advancements in tissue engineering technology and stem cell biology have significantly improved the regenerative reconstruction of alveolar bone defects. The multiple trophic activities of extracellular vesicles (EVs) produced by mesenchymal stem cells play important roles in exerting their therapeutic effects. Several studies have reported the role of dental pulp stem cells (DPSCs) in bone regeneration, but the regenerative effects of DPSC-EVs on alveolar bone defects are unclear. In the present study, the osteogenic effects of DPSC-EVs on Hertwig's epithelial root sheath (HERS) cells *in vitro* and their osteoinductive effects in an alveolar bone defect rat model were investigated. The results showed that DPSC-EVs significantly promoted the expression of osteogenic genes, such as runt-related transcription factor 2 and alkaline phosphatase, and increased the osteogenic differentiation capability of HERS. These findings suggested that transforming growth factor β1 inhibition decreased DPSC-EV-induced Smad, MAPK and ERK phosphorylation in HERS. *In vivo*, DPSC-EV-loaded hydrogels were transplanted into the alveolar sockets of Sprague-Dawley rats and observed for eight weeks. The new bone grew concentrically in the DPSC-EV or DPSC-EV-loaded hydrogel group, with greater bone mass than that in the control group, and the bone volume/total volume increased notably. The results confirmed the osteogenic and osteoinductive effects of DPSC-EVs and DPSC-Exo-loaded hydrogels on alveolar bone defects. Due to their low immunogenicity, high stability, good biocompatibility and osteogenic propensity, DPSC-EV-loaded hydrogels are a safe cell-free therapeutic approach for defective alveolar bone regeneration.

Correspondence to: Professor Dong-Liang Zhang, Department of Orthodontics, School of Stomatology, Beijing Stomatological Hospital, Capital Medical University, 11 Xilahutong Road, Beijing 100040, P.R. China
E-mail: zhangdongliang@mail.ccmu.edu.cn

Dr Kai Yang, Prenatal Diagnosis Center, Beijing Obstetrics and Gynecology Hospital, Capital Medical University, 251 Yaojiayuan Road, Beijing 100040, P.R. China
E-mail: yk19830919@ccmu.edu.cn

*Contributed equally

Key words: alveolar bone defects, extracellular vesicles, dental pulp stem cells, hydrogel, transforming growth factor β1, bone regeneration

Introduction

Several factors, such as congenital malformation of the cleft lip and palate, drug treatment, local inflammation, periodontitis, traumatic injury, malignant tumors and dental surgery, can cause alveolar bone defects (1). Repairing alveolar bone injury or periodontal soft tissue injury is a complex process (2). Due to its favorable osteogenesis and osteoinduction characteristics, autogenous bone transplantation is commonly performed for treating alveolar bone defects (2). However, autologous bone transplantation depends on the donor site conditions, transplantation failure rate and immune rejection of patients (3). Furthermore, the sources of autologous bone grafts are limited, the treatment is painful and the donor site is damaged (3). Other bone tissue substitutes, such as xenotransplantation, are available. However, this approach is hindered by immune rejection and high pathogen transmission (4). Due to the poor integration with natural bone tissue, synthetic grafts often result in graft failure. Therefore, the application of synthetic grafts is limited (5). A suitable technique needs to be developed to fully regenerate damaged bone tissues.

The main aim of repairing alveolar bone defects is to stimulate or induce osteogenic potential and provide the materials, space and environment needed for osteogenesis (6). Hertwig's epithelial root sheath (HERS) is a double-layer epithelial structure formed by the fusion of the inner and outer enamel epithelia in the tooth neck after the formation of the tooth crown during tooth development (7). It differentiates into cementoblasts through epithelial-mesenchymal transition (EMT) and promotes the differentiation of medial

dental papilla cells (DPCs) into odontoblasts through epithelial-mesenchymal interaction, thus secreting and producing dentin from the tooth root (7). Furthermore, HERS can differentiate into cementum cells through EMT and secrete cementum to form periodontal tissue (8). The cementum is formed by differentiating cementoblasts, which have similar phenotypes to osteoblasts, and expresses proteins such as runt-related transcription factor 2 (RUNX2), bone sialoprotein (BSP) and alkaline phosphatase (ALP) (9). The sources of the differentiation of cementum may be dental follicle cells and epithelial cells (7). Considering that the inner cells of HERS initiate the differentiation of odontoblasts to form root dentin, HERS is necessary for root development. For example, if the continuity of HERS is damaged, it cannot induce DPCs to differentiate into odontoblasts, resulting in dentin defects (10). Additionally, if the epithelial root sheath fails to break at a specific time and adheres to the root dentin surface, the dental follicle cells cannot differentiate into cementoblasts to form cementum (11).

Several studies have suggested that extracellular vehicles, including microvesicles and exosomes produced by mesenchymal stem cells (MSCs) and dental pulp stem cells (DPSCs), promote their therapeutic potency by mediating cell-cell communication and transporting paracrine factors to facilitate angiogenesis, immune regulation and tissue regeneration (12,13). Some studies have shown that DPSCs can secrete various molecules in the medium that can be used in regenerative medicine (14,15). Extracellular vesicles (EVs), which are small endocytic vesicles, have attracted attention in bone regeneration research (16). Researchers have found that after coculturing EVs derived from MSCs with chondrocytes, CD73-mediated adenosine activation of AKT and extracellular regulated protein kinase (ERK) signaling in EVs derived from MSCs promotes cell migration, proliferation and matrix synthesis during cartilage repair (17). The implantation of EVs into an animal defect model can significantly increase the number of chondrocytes and heal cartilage defects (18). Although the majority of preliminary studies indicate that EVs stimulate osteogenesis and angiogenesis (18,19), the exact mechanism remains unelucidated. Therefore, reliable methods need to be developed to identify and purify EVs. Exosomes are formed by the multivesicular division of cells and have high therapeutic potential (19). However, they neither self-replicate nor cause autoimmune reactions in the host (19). These paracrine factors can be encapsulated in biomaterials to maintain their biological activity and can undergo controlled release (20). Among the different types of biomaterials studied for the infusion of EVs, hydrogels are the most user-friendly, cost-effective and accessible material (21). Therefore, in the present study an alveolar bone defect model was used to study the osteogenic effects of DPSC-EV-loaded hydrogels with the aim to propose a new strategy for the osteogenic potential of DPSC-EVs for safe cell-free therapy and regeneration of defective alveolar bone.

Materials and methods

Animals. A total of 24 male Sprague-Dawley (SD) rats (age, 10 weeks old; weight, 200±10 g) purchased from Beijing Weitong Lihua Biotechnology Co., Ltd. (cat. no. SCXK-2021-0006) were used in the present study. The rats had free access to food and water. All experimental manipulations were performed in accordance with the National Institute of Health Guide for the Care and Use of Laboratory Animals. All animals were housed in separate cages at the Beijing MeDeKanNa (MDKN) Biotechnology Co., LTD. (experimental animal use license no. SYXK-2020-0050), with an ambient temperature of 20-23˚C, a relative humidity of 60% and under a 12 h light-dark cycle. Animals were fed in the animal room for 7 days before conducting experimental modeling. The animal treatment groups were as follows: i) Alveolar bone injury group (n=6); ii) alveolar bone injury + EV intervention group (100 μg; n=6); iii) alveolar bone injury + EV hydrogel intervention group (100 μg; n=6); and iv) alveolar bone injury + EV hydrogel intervention group (100 μg) + TGF-β1 inhibitor (gavage, 20 mg/kg; three times/week) group (n=6). The present study was approved by The Animal Welfare Ethics Committee of Beijing MDKN Biotechnology Co., LTD. (approval no. MDKN-2022-052; Beijing, China).

Animal alveolar bone defect model. Numerous studies have selected the rat alveolar bone defect model (22-25). In the present study, the rat mandible was lifted to expose its maxillary dentition. Under sterile conditions, a pointed scalpel was used to cut the mesiopalatal gingiva of the first maxillary molar, the gingival flap was gently opened, the mesioalveolar bone surface of the first molar was exposed, and a dental cylindrical needle (diameter, 1.5 mm) was used to remove the mesioalveolar bone of the mesiomedial root of the first maxillary molar in the rats. Intermittent grinding was performed and water was sprayed on the alveolar bone. Finally, a large ball drill (diameter, 4 mm) was used to repair the hole pattern, and was made to meet the surgical standard of a hemispherical defect with a diameter of 4 mm and volume of 16.76 mm^3. Eventually, a buccal alveolar bone was formed at the first to third mandibular molars, forming an ~12 mm^3 bone defect rat model. After the surgery, treatment with EVs, and a rehabilitation membrane (HealAll®; Yantai Zhenghai Bio-Tech Co., Ltd.) was used to cover the alveolar bone defect site to prevent the impact of other connective tissue. The rats were euthanized with CO_2 at a volume displacement of 30% vol/min. After euthanasia, indicators such as breathing, heartbeat, pupils and nerve reflexes were observed to confirm animal death.

Isolation and culture of HERS Cells. In the present study, the rats (n=15) were euthanized, disinfected with 75% ethanol and their mandibles were separated. Under a stereomicroscope, the first mandibular molar embryos were separated via microscopic forceps. A total of ~1-mm thick dental neck tissue was cut along the mineralized edge of the crown, the separated dental neck tissue was rinsed twice with PBS, cut into small pieces (1x1 cm), and digested at 37˚C for 1 h in a mixture of type I collagenase and dispase enzymes. The epithelial culture medium (ScienCell Research Laboratories, Inc.; cat. no. 4101) was added to stop the digestion, the mixture was centrifuged at 250 x g at 4˚C for 5 min to remove the supernatant and the cells were washed with PBS for 5 min twice. Subsequently, the supernatant was removed, the cells were resuspended in epithelial culture medium (ScienCell Research Laboratories, Inc.; cat. no. 4101), the mixture was

inoculated in a 25 ml culture flask and cultured at 5% CO_2 and 37˚C, with the medium changed every two days. On the third day after inoculation, the epithelial cells were purified when they reached a growth rate of ~70%. The culture medium was discarded, and the cells were washed once with PBS. After which, 0.5 ml of 0.25% trypsin EDTA was added, and the cells were placed in a 37˚C incubator for 3 min. When the spindle-shaped cells were observed to shrink under the microscope, 2 ml serum-containing culture medium (Gibco; Thermo Fisher Scientific, Inc.; cat. no. 16000-044) was added to terminate digestion. The medium was gently aspirated to remove the shrunken cells, the medium was discarded and 5 ml epithelial medium (Lifeline Cell Technology; cat. no. LL-0023) was added for further cultivation at 37˚C. After three days, the aforementioned purification step was repeated once, and purified P1-generation HERS epithelial cells were obtained.

DPSC isolation. The surface of the teeth was disinfected and sterilized with 75% ethanol, and the pulp was removed under sterile conditions. After rinsing the dental pulp in sterile phosphate buffered saline (PBS), the pulp was cut into 1.0 mm^3 fragments in α-MEM culture medium (Gibco; Thermo Fisher Scientific, Inc.; cat. no. BC-M-042). A total of 0.5 ml each of 0.3% type I collagenase and 0.4% neutral protease (dispase) was added, and the centrifuge tube containing the dental pulp and digestive fluid was gently shaken to ensure full contact between the dental pulp and digestive fluid. Pieces of dental pulp were digested at 37˚C for 30 min until the tissue mass became loose. After which, an equal volume of α-MEM culture medium containing 20% fetal bovine serum (FBS; Gemini Bio Products; cat. no. 900-108) was added to terminate digestion. The cell precipitate and tissue mass were gently blown and beaten, centrifuged at 100 x g at 4˚C for 6 min and the supernatant was discarded. An appropriate amount of α-MEM culture medium containing 20% FBS was added to the cell precipitate, and gently blown and beaten until a single-cell suspension was mixed with the loose tissue mass. The samples was inoculated into a 25 cm^2 culture bottle, where it was evenly dispersed and spread flat at the bottom of the bottle and incubated in a 37˚C cell incubator. During the first week of adherent culture, to prevent tissue blocks from floating, moving the culture bottle was avoided. The fluid was changed once a week before cell growth and once every 3 days after growth. When the growth of the dental pulp cells reached 80% confluence, the passage was performed using α-MEM culture medium containing 20% FBS, 1% penicillin streptomycin, and 1% glutamine. The samples was cultured in a moist incubator at 37˚C with 5% CO_2, and the culture medium was changed every 3 days. Third-generation dental pulp cells were used for the subsequent experiments.

Collection of extracellular vesicles. DPSCs were inoculated in a 10 cm culture dish. When cell growth reached 80% density, the samples were washed with PBS and the medium was replaced with α-MEM without FBS (Gibco; Thermo Fisher Scientific, Inc.; cat. no. BC-M-042). After 48 h, 180 ml supernatant was collected and centrifuged at 300 x g at 4˚C for 10 min, at 2,000 x g at 4˚C for 10 min and at 10,000 x g at 4˚C for 30 min to remove dead cells and cell fragments. Subsequently, the samples were filtered through a 0.22 μm filter and centrifuged at 100,000 x g for 70 min at 4˚C. After removing the supernatant, vesicles were resuspended with PBS and centrifuged again at 100,000 x g at 4˚C for 70 min (26,27). Extracellular microspheres were resuspended in PBS and frozen at -80˚C for subsequent use.

Detection of extracellular vesicles. The following steps were performed for detecting EVs: i) Glutaraldehyde fixation of EVs; ii) cleaning: the samples were washed three times with 1 ml PBS and left undisturbed for 15 min each time; iii) Acid fixation: 0.5 ml of 2% acid solution was added, and the mixture was incubated at 37˚C for 2 h for fixation; iv) Cleaning: The samples were washed three times with PBS; v) Dehydration: Gradient dehydration with 50, 70, 80 and 90% ethanol was used at 37˚C for 15 min, and then, 100% ethanol was used for dehydration; vi) Replacement: The mixture was replaced with 1 ml acetone twice; vii) Impregnation: The sample was soaked in a suitable resin (Araldite; cat. no. GY250) for electron microscopy observation after curing; viii) Embedding: The samples were placed in an embedding plate containing Leica embedding agent (Leica Biosystems; cat. no. 14020108926); ix) Polymerization: The embedded plate was polymerized at 65˚C for 48 h; x) Staining: The samples were stained with uranium dioxide acetate at 37˚C for 10 min and cleaned; then, the samples were dyed with lead acetate at 37˚C for 10 min and washed; and xi) Electron microscopy examination was performed.

EV concentration detection. EVs were collected and their concentration was measured using a BCA protein concentration assay kit, followed by concentration treatment. The optical density was measured using a microplate reader (SpectraMR; Dynex) at 562 nm. A standard curve was drawn based on the absorbance and concentration of the standard sample, and the protein concentration was calculated.

Nanoparticles tracking analysis (NTA) of EVs. To observe the particle size distribution, nanoparticles tracking analysis (NTA) of the isolated DPSCs-EVs was implemented. A total of 20 μg DPSCs-EVs were uniformly dispersed in 1 ml PBS, followed by analysis by the NanoSight nanoparticle tracking analyzer (Malvern Panalytical, Ltd.). The sample was agitated on a vortex mixer for 5-10 sec, a 2.5 ml syringe was used to aspirate the sample, it was inverted 2-3 times. The samples were slowly injected and the interface particles were observed.

Immunofluorescence confocal microscopy. Purified P1-generation HERS epithelial cells were obtained. HERS cells were plated in 96-well flat bottom plates at a density of $2x10^5$ cells/well. After treatment with DPSC-derived EVs with a concentration of 20 μg/ml at 37˚C for 24 h, the HERS cells were washed thrice with PBS, and fixed with 4% paraformaldehyde in PBS at 37˚C for 20 min. The cells were then permeabilized with 0.3% Triton X-100 at 37˚C for 5 min. The sections were pre-blocked with 5% bovine serum albumin (MilliporeSigma; cat. no. A7030-5G) in PBS at 37˚C for 30 min and stained with the following primary antibodies: Anti-E-cadherin (Proteintech Group, Inc.; cat. no. 20874-1-AP; 1:200), anti-vimentin (Novus Biologicals,

Ltd.; Bio-Techne; cat. no. NB300-223SS; 1:200) and anti-cytokeratin 14 (CK14) antibody (Proteintech Group, Inc.; cat. no. 10143-1-AP; 1:200) overnight at 4˚C. After being washed in PBS thrice, the HERS cells were stained with 488-conjugated AffininPure Goat Anti-Mouse IgG (H+L; Jackson ImmunoResearch Laboratories, Inc.; cat. no. 115-545-003) and 594-conjugated AffiniPure Donkey Anti-Rabbit IgG (H+L; Jackson ImmunoResearch Laboratories, Inc.; cat. no. 711-585-152) overnight at 4˚C followed by washing with 3X PBS. After washing, the nuclei were stained with Heochst (Sigma-Aldrich; Merck KGaA) at 37˚C for 5 min. Finally, the cells were observed using a laser-scanning confocal microscope (Leica Microsystems GmbH).

Cell counting kit-8 (CCK-8) assay. HERS cells were plated in 96-well flat bottom plates at a density of $2x10^5$ cells/well and incubated with PBS and exosomes in a medium containing 10% fetal calf serum (FCS; Gibco; Thermo Fisher Scientific, Inc.; cat. no. 10099-141) at 37˚C in 5% CO_2 in humidified air for 48 h. After which, 10 μl CCK-8 solution (Dojindo Laboratories, Inc.) was added to each well for 2 h. The optical density was measured using a microplate reader (SpectraMR; Dynex) at 540 nm.

Western blotting. Protein concentrations were measured using a BCA protein assay kit (Thermo Fisher Scientific, Inc.). A total of 100 μg of the total protein was loaded per well. The proteins in the HERS cells were separated via 10-12% sodium dodecyl sulfate-polyacrylamide gel electrophoresis (Beijing Solarbio Science & Technology Co, Ltd.; cat. no. P1200) and transferred electrophoretically onto an immobilon polyvinylidene difluoride membrane. After blocking with 10% skim milk overnight at 4˚C, the membrane was incubated for 6 h at room temperature with anti-BSP (CST Biological Reagents Co., Ltd.; cat. no. 5468), anti-ALP (Abcam; cat. no. ab229126), anti-RUNX2 (CST Biological Reagents Co., Ltd.; cat. no. 12556), anti-TGF-β1 (Abcam; cat. no. ab315254), anti-TGFR1 (Abcam; cat. no. ab235578), anti-Smad2/3 (Abcam; cat. no. ab202445), anti-phosphorylated (p-)Smad3 (Abcam; cat. no. ab202445), anti-MAPK (Abcam; cat. no. ab308333), anti-ERK (Abcam; cat. no. ab184699), anti-p-ERK (Abcam; cat. no. ab314200), anti-CD9 (Abcam; cat. no. ab307085), anti-CD63 (Abcam; cat. no. ab108950), anti-CD81 (Abcam; cat. no. ab155760), anti-TSG101 (Abcam; cat. no. ab125011), anti-Calnexin (Abcam; cat. no. ab22595) and anti-GAPDH (Proteintech Group, Inc.; cat. no. 6004-1-1g) antibodies (all 1:1,000). The TBST buffer (TBS buffer containing 0.05% Tween-20) was prepared and the membrane was washed three times with 1X TBST. After which, the membrane was incubated with HRP-labeled Goat Anti-Rabbit IgG H&L antibody (Abcam; cat. no. ab205718; 1:2,000) for 1 h at room temperature. The membrane was washed again three times with TBST and developed via an enhanced chemiluminescence (ECL) plus chemiluminescence kit (Tanon Science & Technology, Co., Ltd.; cat. no. 180-501). Protein bands were detected using an Odyssey System (LI-COR Biosciences).

ALP staining. The aforementioned grouped cells were cultured at 37˚C in 5% CO_2 in humidified air for 48 h, the supernatant was discarded, washed twice with PBS, and fixed with 70% alcohol at 37˚C for 2 min. Distilled water was used to remove the fixative. Using alkaline phosphatase calcium cobalt staining kit (Jiangsu Kaiji Biotechnology, Co., Ltd.; cat. no. KGA353), incubation solution A and B were mixed to form the incubation working solution before use. The sample was incubated with the incubation solution at 37˚C for 3 h. The sample was then rinsed with water for 5-10 min. After which, the sample was incubated with staining solution A at room temperature for 5 min and rinsed with water for 2 min. Then, the sample was incubated with staining solution B at room temperature for 1 min and rinsed again for 5 min. Images were captured using a biological inverted microscope (Olympus Soft Imaging Solutions GmbH; cat. no. IX71).

Alizarin Red staining determination. The medium was changed every 3 days, and after 14 and 21 days the culture medium was aspirated. The samples was washed twice with PBS, fixed with 4% paraformaldehyde for 30 min at 37˚C and washed with deionized water. After which, the sample was stained with 2% Alizarin Red staining solution for 20-30 min at 37˚C, and images were captured with a fluorescence microscope. After which, decolorization treatment was performed, whereby 200 μl 5% perchloric acid solution was added to each well, the sample was gently agitated on a shaker for 15 min and then transferred with 150 μl decolorization solution to a 96 well plate. The sample was read with an enzyme-linked immunosorbent assay reader, the OD value was recorded and detected at a wavelength of 490 nm.

Flow cytometry analysis. Cells were seeded in a 96-well culture plate, and the number of cells in each well was adjusted to $1x10^5$ using 10% FCS-RPMI 1640 medium (Thermo Fisher Scientific, Inc.; cat. no. 22400089), with a final volume of 200 μl/well. A portion from each group of cells was extracted for flow cytometry detection of CD44, CD34, CD45 and CD90. The cells were washed with pre-cooled PBS and resuspended in 100 μl PBS. Anti-CD44-PE (Abcam; cat. no. ab23396), anti-CD34-PE (Abcam; cat. no. ab223930), anti-CD45-PE (eBioscience; cat. no. 12-0451-83) and anti CD90-PE (Abcam; cat. no. ab33694) was added to the samples and incubated at 4˚C in the dark for 30 min. The cells were washed twice with 2 ml 1X transmembrane buffer, suspended in PBS and detected by flow cytometry (BD Biosciences, C6 model), and analyzed by the Cytek® NL-CLC full spectrum flow cytometer.

Transmission electron microscopy (TEM). The isolated exosomes were evaluated using transmission electron microscopy (TEM). Firstly, 10 μl of each sample was dropped onto a 200 mesh ultra-thin carbon coated copper grid at 37˚C for 2 min. After which, the grid was quickly dried on filter paper. Negative staining was performed on the grid using 1% uranyl acetate (filtered twice through a 0.22 μm filter). After complete drying for 1 min, images were captured using Hitachi HT-7700 TEM at a voltage of 100 kV.

Reverse transcription-quantitative polymerase chain reaction (RT-qPCR). Third-generation HERD cells were seeded in 6-well plates at a density of $1x10^4$ cells/well and co-cultured at 37˚C with osteogenic medium (ScienCell Research Laboratories, Inc.; cat. no. YB4601) and scaffolds for 14 and

Table I. Primer sequences for RT-qPCR.

Primer	Sequence (5'-3')
Rattus GAPDH_F	GCTGAGTATGTCGTGGAGTC
Rattus GAPDH_R	GATGCATTGCTGACAATCTT
Rattus BSP_F	CGGCCACGCTACTTTCTTTA
Rattus BSP_R	CTCCAACTTTCCAGCGTCA
Rattus RUNX2_F	CCTATGACCAGTCTTACCCC
Rattus RUNX2_R	CAGAGGCAGAAGTCAGAGGT
Rattus ALP_F	CGGCTATGAACAGTGTGATG
Rattus ALP_R	ACCGCGTTCCAGACAGTAG
Rattus TGF-β1_F	CGCCTGCAGAGATTCAAGT
Rattus TGF-β1_R	CTCGACGTTTGGGACTGAT
Rattus ERK1/2_F	GAACATCATCGGCATCAATG
Rattus ERK1/2_R	TGAGGTCACGGTGCAGAA
Rattus p38 MAPK_F	ACATCGTGTGGCAGTGAAGA
Rattus p38 MAPK_R	ACGTGGTCATCGGTAAGCTT
Rattus Smad3_F	GGCTACCTGAGTGAAGATGGA
Rattus Smad3_R	GGCTGTAGGTCCAAGTTATTG
Rattus TGFβR1_F	TCACTAGATCGCCCTTTCAT
Rattus TGFβR1_R	TCGCCAAACTTCTCCAAAC

F, forward; R, reverse; BSP, bone sialoprotein; RUNX2, runt-related transcription factor 2; ALP, alkaline phosphatase.

21 days to obtain cell pellets. Total RNA was extracted with TRIzol® reagent (Invitrogen; Thermo Fisher Scientific, Inc.), and cDNA was synthesized using the PrimeScript RT Master Mix Perfect Real-Time Kit at 37˚C (Takara Biotechnology, Co., Ltd.). The relative gene expression level was normalized with the internal parameter (GAPDH). The reaction procedure was: 30 sec at 95˚C, and 40 cycles of 5 sec at 95˚C, 30 sec at 60˚C. SYBR Select MasterMix (Takara) was used for q-PCR assay to detect mRNA levels of ALP, BSP, RUNX2, TGF-β1, TGFR1, Smad2/3, MAPK and ERK1/2. All primers used in the present study were purchased from GeneChem, Inc., (Table I).

Micro-CT analysis. SD rats in each group (n=6) were anesthetized with 3% pentobarbital sodium (50 mg/kg; intraperitoneally). After which, a micro-CT system was used to calculate the bone mineral density (BMD) and the bone volume/total volume (BV/TV) ratio of regenerated bone in the calvarial defect. The CT Analyzer (version 1.20.3.0; Bruker Corporation) was used to analyze the region of interest. Unified parameters were set to calculate the TV, BV, BV/TV, bone area (BS), number of trabeculae (Tb. N) and thickness of trabeculae (Tb. th) of the tissue. The micro-CT equipment was set with a tomographic rotation of 180˚ at 85 kV and 135 mA.

Statistical analysis. Statistical analyses were performed using the GraphPad Prism 9.0 software (Dotmatics). The data were presented as the mean ± standard deviation (SD). Data were consistent with a normal distribution based on the Shapiro-Wilk test. One-way ANOVA combined with Tukey's post-hoc test were employed for the comparison of statistical difference. $P<0.05$. was considered to indicate a statistically significant difference.

Results

Identification of DPSC-EVs and validation of uptake experiments. First, the morphology of DPSCs was observed and first generation DPSCs cells (P1) were shown to be short and irregularly shuttle-shaped, while the third generation DPSCs cells (P3) appeared to be long and regularly shuttle-shaped (Fig. 1A). DPSCs and DPSC-EVs were isolated. The results of the flow cytometry assays with DPSC markers showed positive expression of CD44 and CD90 and negative expression of CD34 and CD45 (Fig. 1B). Alizarin red, ALP and Oil red O staining in DPSCs was also performed and the results showed that Alizarin red staining could clearly display calcified plaques (Fig. 1C) and ALP was expressed in DPSCs. Next, the morphology of the EVs via TEM was observed (Fig. 1D), and the NTA particle size was determined to be 115 nm (Fig. 1E). The results of the western blotting analysis revealed that the extracellular vesicle markers CD9, CD63, TSG101 and CD81 were expressed, whereas, the DPSC marker calnexin was not expressed (Fig. 1E).

The HERS cells were isolated and co-cultured with DPSC-EVs, and immunofluorescence staining was used to detect epithelial cell markers, including CK14 and Vimentin. Immunofluorescence staining showed CK14 and Vimentin were expressed in the HERS cells (Fig. 2A). The uptake of EVs was assessed via confocal microscopy. The EVs were stained with green fluorescence. The range of green fluorescence staining agents in the EVs in the DPSC-EV group increased, and the color of green fluorescence became increasingly intense, indicating that the number of EVs taken up increased with time. A comparison between the PBS and EV groups revealed nearly no visible exocrine uptake between these two

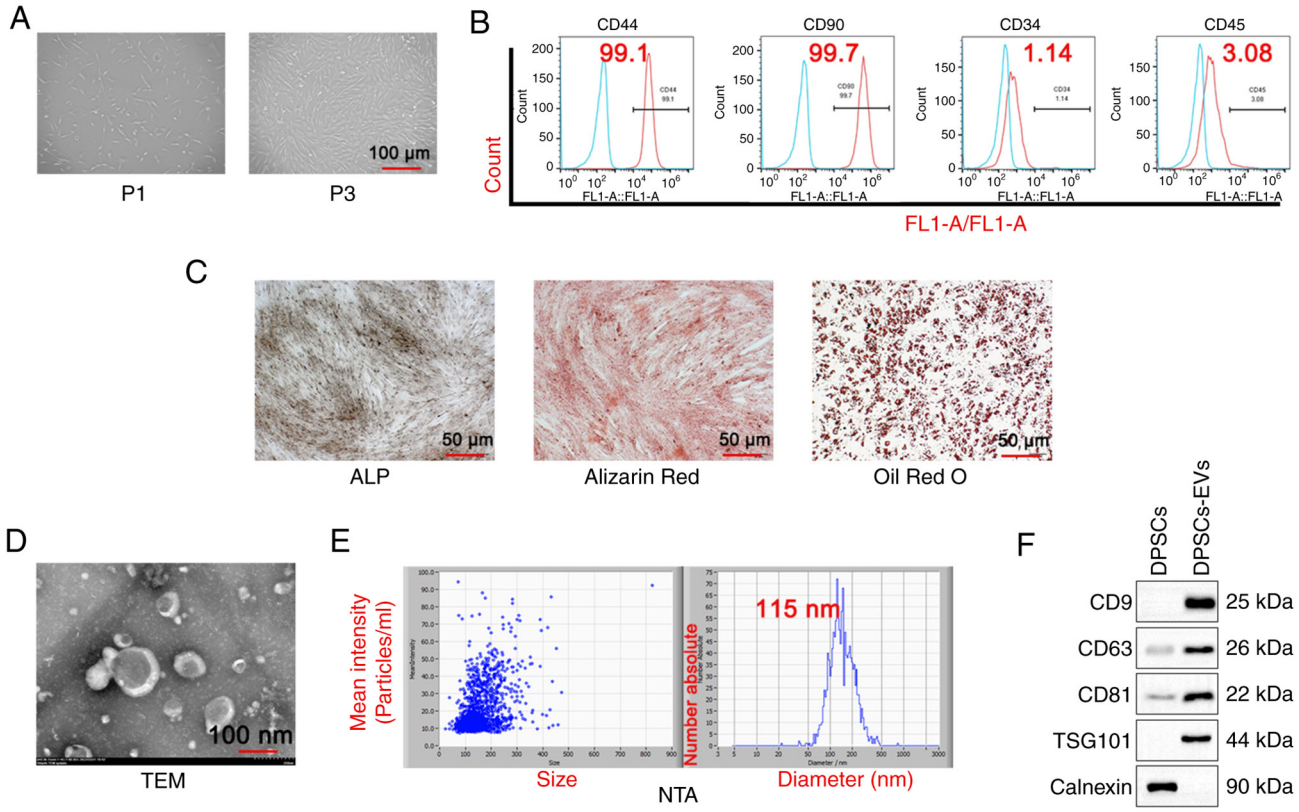

Figure 1. Isolation and identification of DPSC and DPSC-EVs. (A) DPSCs were isolated, cultured and observed under a microscope. (B) Flow cytometry was performed to detect DPSC markers (CD44, CD90, CD34 and CD45). (C) ALP staining, Alizarin red staining and Oil Red O staining were performed to evaluate the osteogenic capacity of DPSCs. (D) The morphological features of DPSC-EVs were observed. The average size of EVs was 115 nm. (E) The NTA particle size of DPSC-EVs was analyzed. (F) Western blotting was performed to detect DPSC-EV markers (CD9, CD63, CD81, TSG101 and calnexin). Triplicate independent experiments were used. DPSC, dental pulp stem cell; EV, extracellular vesicle; NTA, nanoparticles tracking analysis; FL1, green fluorescent channel; P1,first generation DPSCs cells; P3, third generation DPSCs cells; TSG101,tumor susceptibility gene 101; TEM, transmission electron microscopy.

groups at 1 h. Thus, the uptake of EVs commenced after 1 h ($P<0.05$; Fig. 2B). The difference in the quantity of secretions ingested between the two groups increased over time (Fig. 2B). Next, different concentrations (10, 15 and 20 μg/ml) of DPSC-EVs were used to stimulate HERS cells for 12, 24 and 48 h. The results showed that with a concentration of 20 μg/ml at 48 h, compared with control, the cell proliferation activity of HERS increased significantly after treatment with DPSC-EVs ($P<0.05$; Fig. 2C).

DPSC-EVs promote EMT and osteogenic differentiation of HERS cells. To further evaluate the ability of DPSC-EVs to promote the osteogenic differentiation of HERS cells, changes in epithelial and mesenchymal cell markers in HERS cells were detected. After 24 h of coculture with DPSC-EVs and HERS cells, the expression of the epithelial cell marker E-cadherin in HERS cells decreased, whereas the expression of the mesenchymal cell marker vimentin and type I collagen increased compared with control group ($P<0.05$; Fig. 2D). Immunofluorescence staining showed that CK14 expression was increased in the DPSC-EVs group compared with control group ($P<0.05$; Fig. 2E), the expression of E-cadherin in HERS cells decreased in the DPSC-EVs group compared with control group ($P<0.05$; Fig. 2F) and the expression of vimentin in HERS cells increased in the DPSC-EVs group compared with control group ($P<0.05$; Fig. 2G). These findings indicated that HERS cells simultaneously express epithelial and mesenchymal cell markers, with dual characteristics of epithelial and mesenchymal cells, promoting epithelial-to-mesenchymal cell transformation after being stimulated by DPSC-EVs. Therefore, after treatment with DPSC-EVs, HERS cells may differentiate into cementoblasts through EMT.

Furthermore, ALP activity was significantly greater in the DPSC-EV group compared with control group ($P<0.05$; Fig. 3A). Cell mineralization determined via Alizarin red staining revealed that the Alizarin red content in the DPSC-EV groups was significantly greater than that in the control group ($P<0.05$; Fig. 3B). In addition, compared with control group, the expressions of BSP, ALP and RUNX2 were increased significantly in the cells of the DPSC-EV (HERS) group ($P<0.05$; Fig. 3C). mRNA levels of ALP (Fig. S1A), RUNX2 (Fig. S1B), BSP (Fig. S1C), TGFR1 (Fig. S1D), TGF-β1 (Fig. S1E), Smad3 (Fig. S1F), ERK (Fig. S1G) and MAPK (Fig. S1H) were increased significantly in the cells of the DPSC-EV (HERS) group compared with control group. Furthermore, RUNX2 expression in HERS cells was also studied via RUNX2 staining. DPSC-EVs promoted the expression of RUNX2, thus promoting osteogenic differentiation ($P<0.05$; Fig. 3D). Therefore, following DPSC-EV-induction, HERS cells retained osteogenic potential, which indicated that HERS cells can be used for cementum regeneration.

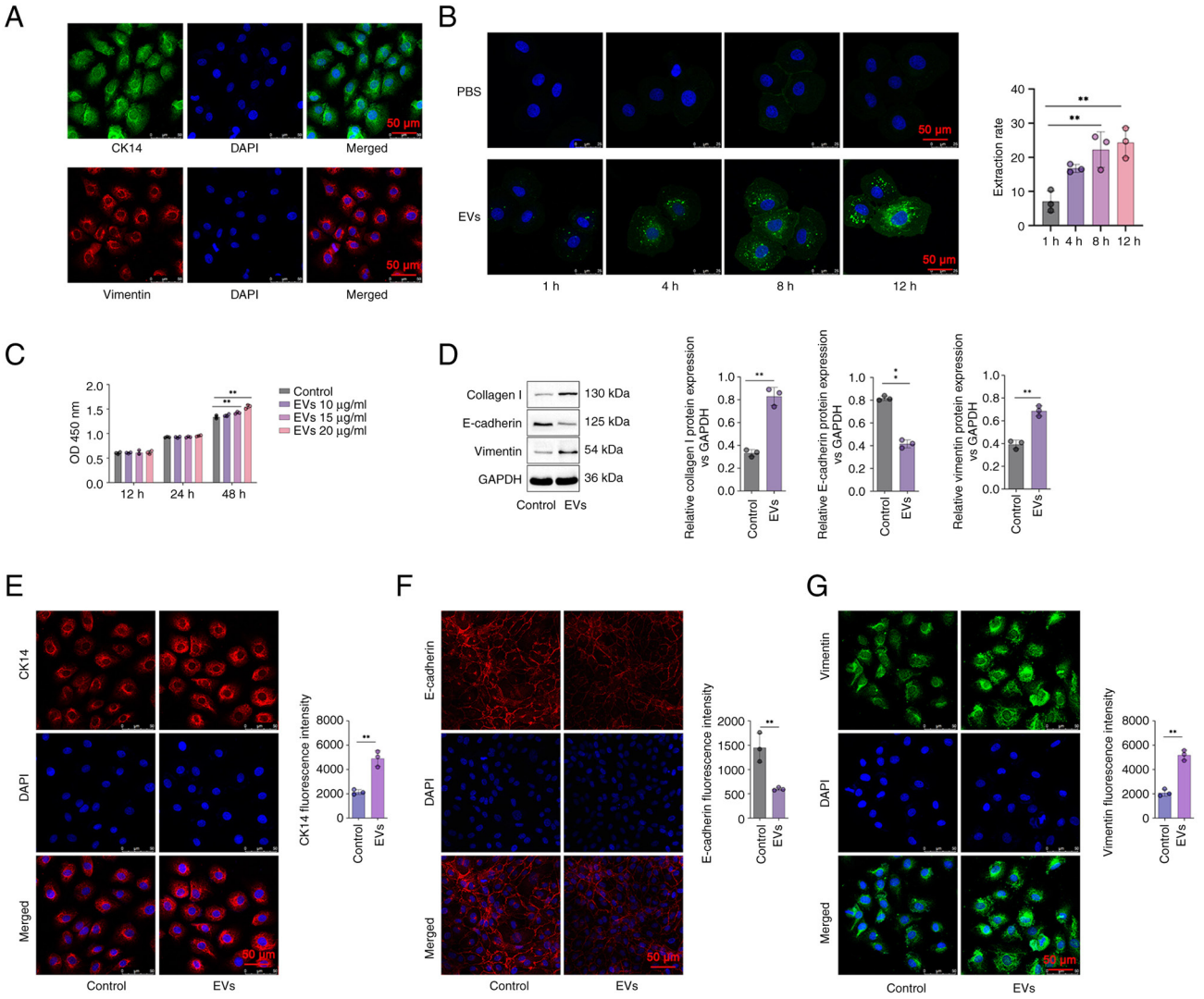

Figure 2. DPSC-EVs promoted EMT in HERS cells. (A) HERS cells were cultured and identified by detection of their markers (CK14 and vimentin) via immunofluorescence staining. (B) HERS cells were co-cultured with DPSC-EVs, and the uptake of DPSC-EVs was monitored via confocal microscopy. (C) HERS cells were co-cultured with different concentrations of DPSC-EVs, and the optimal concentration of DPSC-EVs was determined by performing a CCK-8 assay. (D) The expression of EMT-related proteins (E-cadherin, vimentin and collagen I) in co-cultured HERS cells was detected by Western blotting. (E) The expression of CK-14 in co-cultured HERS cells was assessed by immunofluorescence staining. (F) The expression of E-cadherin in co-cultured HERS cells was assessed by immunofluorescence staining. (G) The expression of Vimentin in co-cultured HERS cells was assessed by immunofluorescence staining. The data from three independent experiments are presented as the mean ± SD. **P<0.01. EMT, epithelial-mesenchymal transition; DPSC, dental pulp stem cell; EV, extracellular vesicle; HERS, Hertwig's epithelial root sheath.

DPSC-EV-induced osteogenic differentiation is regulated by TGF-β1/ERK signaling. The involvement of TGF-β1 in DPSC-EV-mediated osteogenic differentiation was further elucidated. In the present study, the protein levels of TGF-β1, TGFR1, p-Smad3 and MAPK/ERK were determined via Western blotting. The findings revealed that the expression of TGFR1 and TGF-β1were significantly increased in DPSC-EV-treated cells compared with control group (P<0.05; Fig. 3E). Relative expression of p-Smad3/Smad3, ERK/p-ERK and MAPK/p-MAPK were significantly increased in DPSC-EV-treated cells compared with control group (P<0.05; Fig. 3F and G). Using a specific inhibitor of TGF-β1, it was found that ALP expression in the DPSC-EVs + TGF-β1inhibitor group was lower than that in the DPSC-EV group (Fig. 4A), and ALP activity was also significantly lower in the DPSC-EV + TGF-β1 inhibitor group compared with DPSC-EV group (P<0.05; Fig. 4B). Using a specific inhibitor of TGF-β1, the Alizarin red content in the DPSC-EVs + TGF-β1 inhibitor group was lower than that in the DPSC-EV group (Fig. 4C), and Alizarin red expression was also significantly lower in the DPSC-EV + TGF-β1 inhibitor group compared with the DPSC-EV group (P<0.05; Fig. 4D). The confocal microscopy results revealed that TGF-β1 inhibition weakened the positive effect of DPSC-EVs on the expression of RUNX2 (P<0.05; Fig. 4E). It was also found that treatment with a TGF-β1 inhibitor reversed the increase in the expression of TGFR1 and TGF-β1 induced by DPSC-EVs (P<0.05; Fig. 4F). The levels of MAPK, ERK, Smad3 and p-Smad3 were detected by Western blotting (Fig. 4G), and were increased in the DPSC-EVs group compared with control group, and consistently lower in the TGF-β1 inhibitor-treated group than in the DPSC-EVs group (all P<0.05, Fig. 4H). Furthermore, mRNA levels of TGF-β1 (Fig. S2A), TGFR1 (Fig. S2B), Smad3 (Fig. S2C), MAPK (Fig. S2D) and ERK (Fig. S2E) in

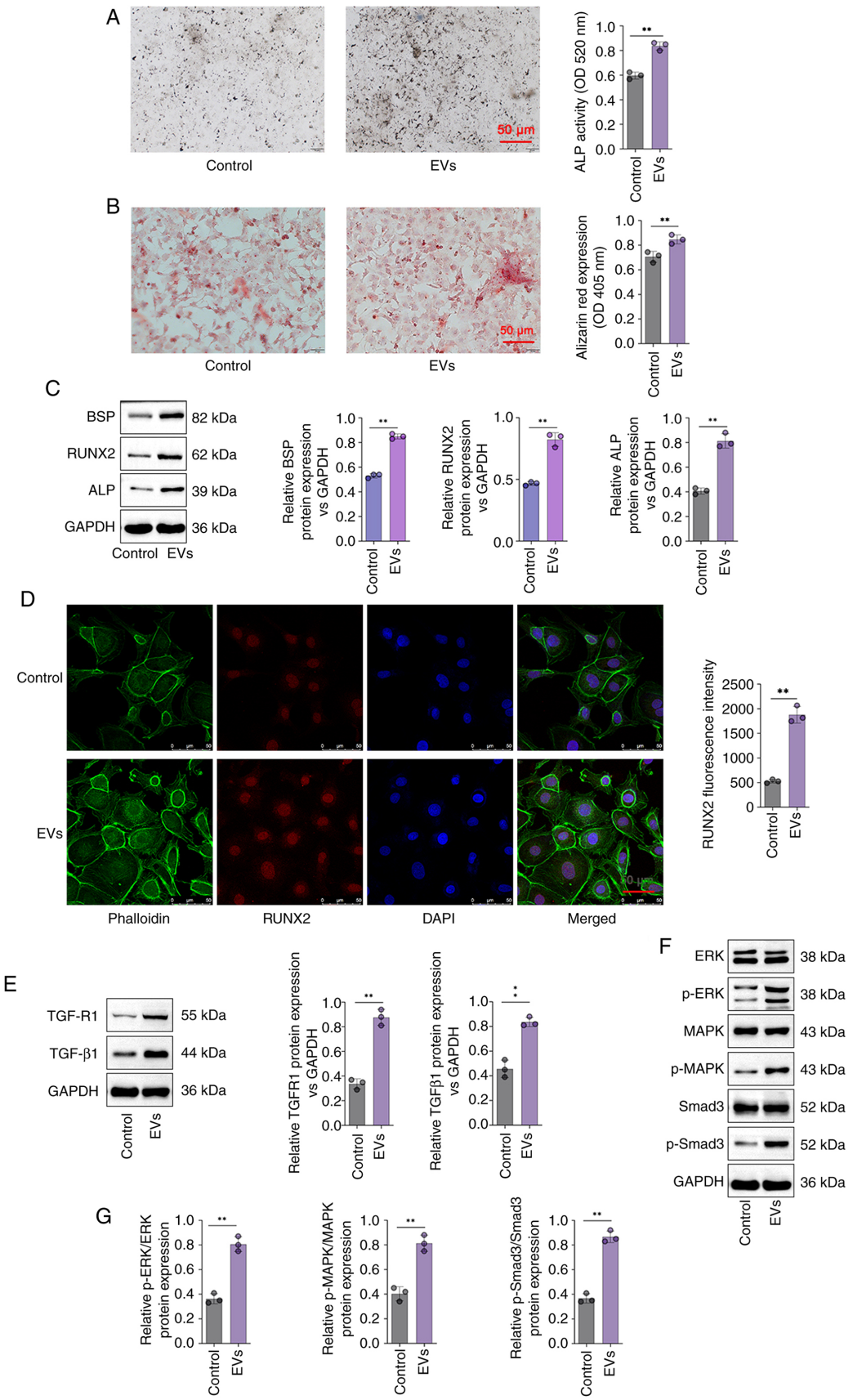

Figure 3. DPSC-EVs promoted the osteogenic differentiation of HERS cells and activated TGF-β1/ERK signaling. (A) ALP staining and (B) Alizarin red staining of HERS cells were conducted to detect their osteogenic capacity. (C) The expression of osteogenesis-related proteins (BSP, ALP and RUNX2) in HERS cells was detected by Western blotting to evaluate their osteogenic capacity. (D) RUNX2 expression in HERS cells was detected via RUNX2 immunofluorescence staining. (E) The expression of TGF-β1 and TGFR1 in HERS cells was detected via Western blotting. (F) ERK/MAPK/Smad signaling activity in HERS cells was evaluated via Western blotting. (G) Relative protein levels of P-ERK/ERK, p-MAPK/MAPK and p-Smad3/Smad3 were analyzed. The data from three independent experiments are presented as the mean ± SD. **P<0.01. DPSC, dental pulp stem cell; EV, extracellular vesicle; HERS, Hertwig's epithelial root sheath; p, phosphorylated; RUNX2, runt-related transcription factor 2; ALP, alkaline phosphatase; BSP, bone sialoprotein.

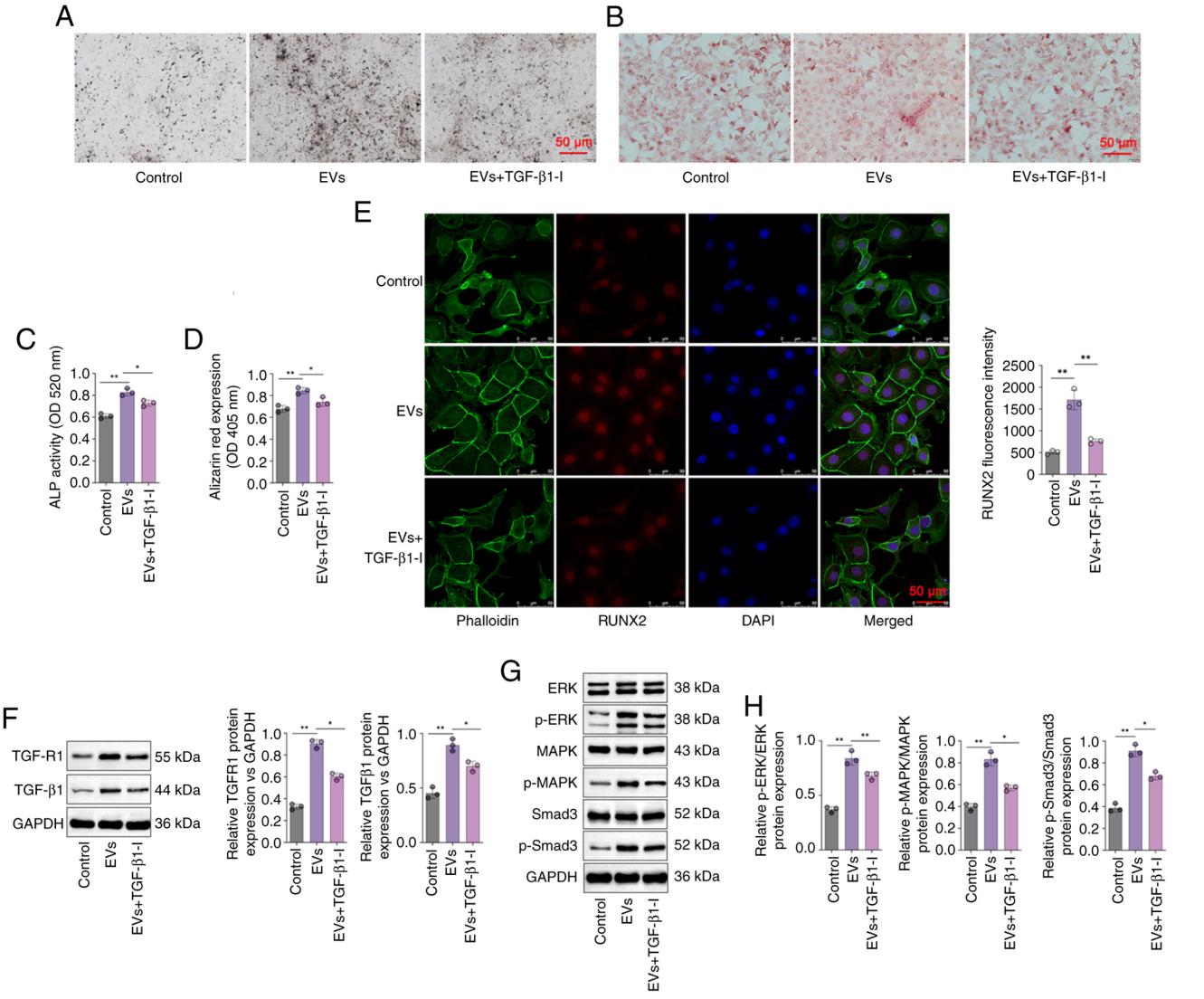

Figure 4. DPSC-EVs may induce the osteogenic differentiation of HERS cells by activating TGF-β1/ERK signaling. (A) ALP staining was performed to evaluate the osteogenic ability of HERS cells. (B) Alizarin red staining was performed to evaluate the osteogenic ability of HERS cells. (C) ALP activity was detected in the HERS cells. (D) Alizarin red expression was detected in HERS cells. (E) Immunofluorescence staining was conducted on HERS cells to monitor the expression of RUNX2. (F) The expressions of TGF-β1 and TGFR1 in HERS cells were determined by Western blotting. (G) The activity of ERK/MAPK/Smad signaling in HERS cells were determined by Western blotting. (H) The expressions of MAPK, ERK, Smad3 and p-Smad3 were increased in the DPSC-EVs group compared with control group. The data from three independent experiments are presented as the mean ± SD; *P<0.05 and **P<0.01. DPSC, dental pulp stem cell; EV, extracellular vesicle; HERS, Hertwig's epithelial root sheath; p, phosphorylated; RUNX2, runt-related transcription factor 2; ALP, alkaline phosphatase.

the TGF-β1 inhibitor-treated group were markedly decreased compared with the EVs only group.

DPSC-EV-loaded hydrogels accelerate bone regeneration in rats with alveolar bone defects. After establishing the alveolar bone defect rat model, micro-CT examinations were first performed to observe bone regeneration in each rat group showing bone regeneration in rats with alveolar bone defects after injecting DPSC-EVs and DPSC-EV-loaded hydrogel (Fig. 5A). New bone grew concentrically in the DPSC-EV and DPSC-EV-loaded hydrogel groups, with greater bone mass in these groups than in the blank control group, and the BV/TV increased significantly compared with control group (Fig. 5B). Furthermore, the effects of DPSC-EVs, DPSC-EV-loaded hydrogel or DPSC-EV-loaded hydrogel and TGF-β1i on osteogenic differentiation in alveolar bone defect model rats were also evaluated using Western blotting (Fig. 5C). The levels of TGF-β1 and p-Smad3/Smad3 were significantly greater in the DPSC-EV-loaded hydrogel group than in the DPSC-EV group; thus, treatment with the TGF-β1 inhibitor decreased the expression of TGF-β1 and p-Smad3/Smad3 (P<0.05; Fig. 5D). Expressions of BSP, ALP and RUNX2 were significantly greater in the DPSC-EV-loaded hydrogel group than in the DPSC-EV group, and the expression of BSP, ALP and RUNX2 were decreased upon treatment with the TGF-β1 inhibitor (P<0.05; Fig. 5E). mRNA levels of ALP (Fig. S3A), BSP (Fig. S3B), RUNX2 (Fig. S3C), TGF-β1 (Fig. S3D) and Smad3 (Fig. S3E) were significantly increased in the DPSC-EV-loaded hydrogel group than in the DPSC-EV group, but were decreased in the TGF-β1 inhibitor group.

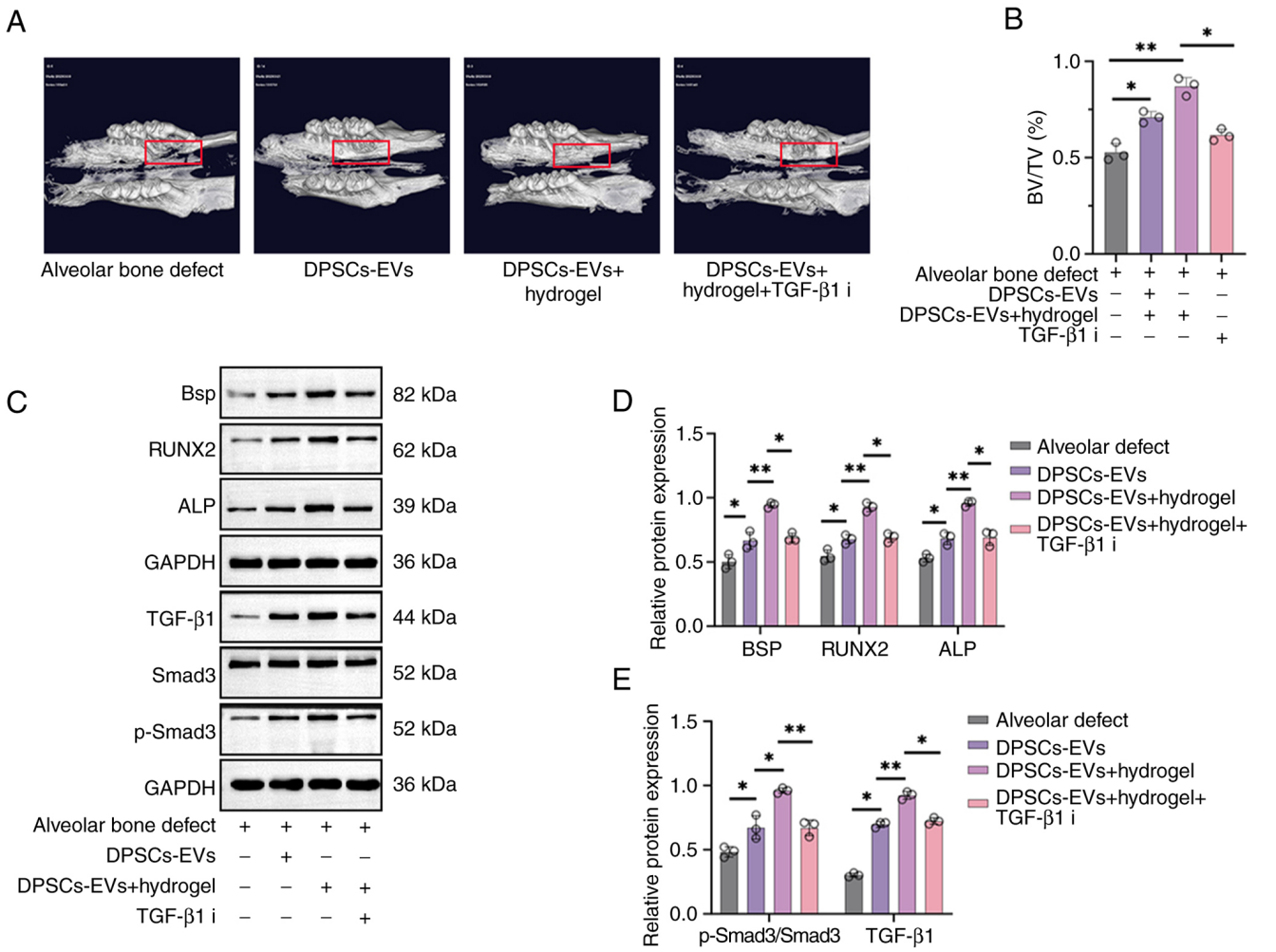

Figure 5. DPSC-EV-loaded hydrogels accelerated bone regeneration in rats with alveolar bone defects. (A) A rat model of alveolar bone defects was established, and the rats were treated with DPSC-EVs. The rats were euthanized after the operation, and new bone regeneration was less intense in the control group and hydrogel group. More new bones were found in the hydrogel + DPSCs-EVs group. (B) Similarly, the BV/TV results showed that the hydrogel + DPSCs-EV group formed more new bones than the other groups. (C) The expression of osteogenesis-related proteins (BSP, ALP and RUNX2) and TGF-β1/Smad signaling were determined via Western blotting. (D) Expressions of TGF-β1 and p-Smad3/Smad3 were significantly greater in the DPSC-EV-loaded hydrogel group than in the DPSC-EV group. (E) Expressions of BSP, ALP and RUNX2 were significantly greater in the DPSC-EV-loaded hydrogel group than in the DPSC-EV group. The data from three independent experiments are presented as the mean ± SD; *P<0.05 and **P<0.01. DPSC, dental pulp stem cell; EV, extracellular vesicle; HERS, Hertwig's epithelial root sheath; p, phosphorylated; RUNX2, runt-related transcription factor 2; ALP, alkaline phosphatase; i, inhibitor; BV/TV, bone volume/total volume; BSP, bone sialoprotein.

Discussion

Bone tissue engineering is an interdisciplinary field that combines the application of osteoblasts (stem cells/progenitors), bioactive molecules and biocompatible scaffolds, as well as, stem cells and signaling molecules (28). The key factors involved in bone tissue engineering are cells, scaffolds and signaling molecules (29). Similar to other bone tissues, osteoclasts and osteoblasts are the primary factors involved in bone formation and bone homeostasis in alveolar bone (30,31). Additionally, a complex cellular communication network plays a key role in maintaining bone coupling and alveolar bone homeostasis (32). However, the invasion of pathogens from the oral environment or blood transmission, orthodontic treatment, drugs and mechanical stress caused by systemic pathological factors induce complex inflammation, which in turn activates osteoclasts and inhibits osteoblasts, thus disrupting the balance between bone removal and regeneration, leading to alveolar bone loss (33-36). In the present study, rat alveolar bone defects model were used and the surgery was carried out as described previously (25). Animals were sacrificed from each group and tissue samples were collected for micro-CT analysis. It was found that DPSC-EVs were highly biocompatible and effectively promoted the proliferation and migration of HERS cells when an appropriate number of DPSC-EVs was used. The DPSC-EV-loaded hydrogel promoted osteogenic and osteoinductive effects in alveolar bone defects in rats.

The present study investigated methods for promoting the interaction between DPSC-EVs and HERS cells. It was found that DPSC-EVs created a dimensional environment conducive to cell growth. The high cell viability in the DPSC-EV culture indicated that DPSC-EVs were biocompatible. DPSC-EVs also promoted the differentiation of HERS cells via EMT. Bone formation is a complex process, and the expression of genes closely related to bone formation in osteoblasts is necessary for the differentiation of osteoblasts into osteoblasts (37);

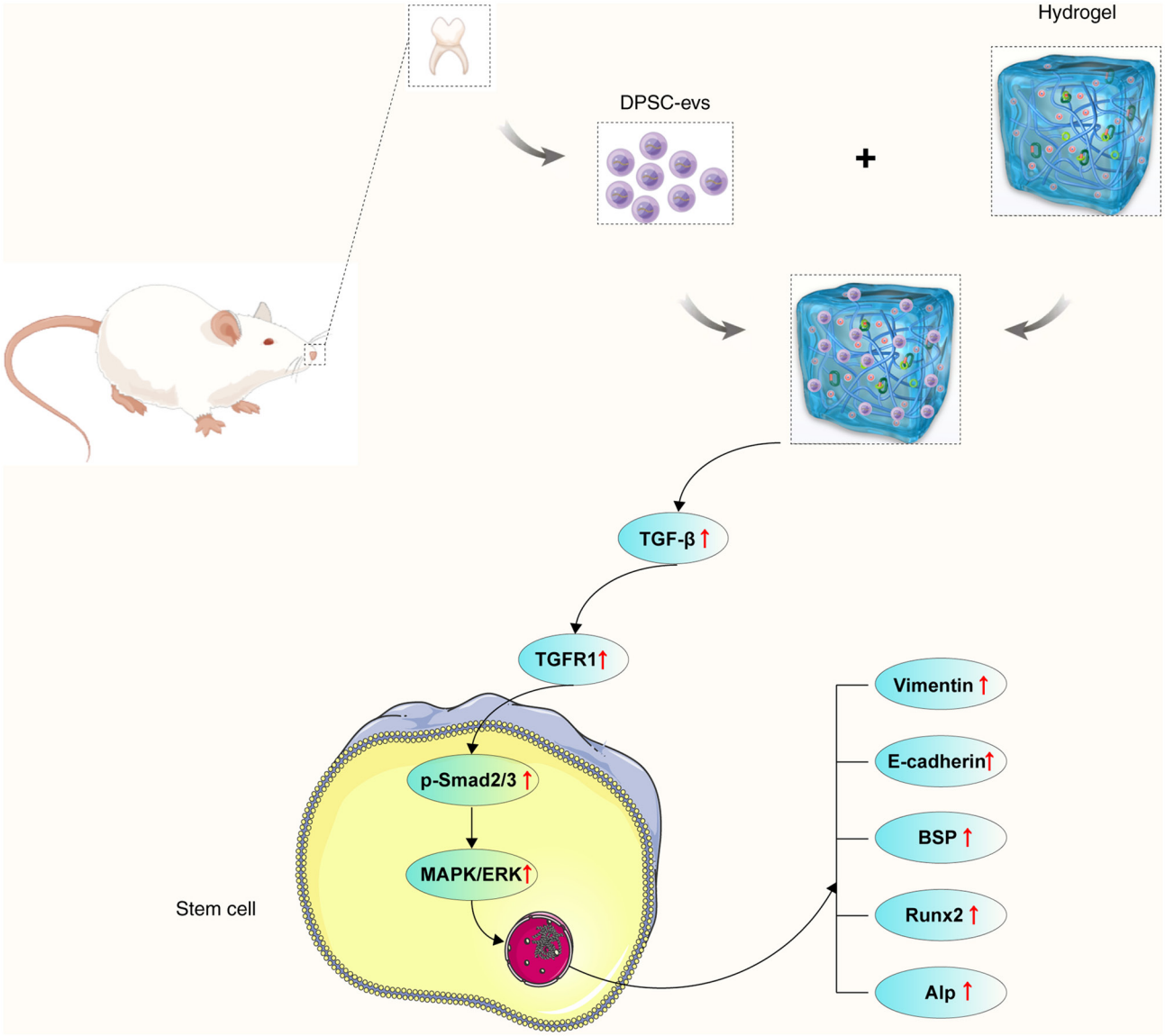

Figure 6. Proposed mechanism of DPSC-derived EVs loaded with hydrogels promote osteogenesis in rats with alveolar bone defects. DPSC-derived EVs loaded with hydrogels promote osteogenesis by ERK/MAPK/Smad signaling in rats with alveolar bone defects. DPSC, dental pulp stem cell; EV, extracellular vesicle; HERS, Hertwig's epithelial root sheath; BSP, bone sialoprotein; RUNX2, runt-related transcription factor 2; ALP, alkaline phosphatase.

such genes are called bone-related genes (38). During *in vivo* bone formation, bone-related gene expression has a strictly regulated time sequence (39). The orderly expression of bone-related genes is crucial for the bone metabolism of osteoblasts, osteogenesis, bone growth and bone reconstruction (40). ALP is produced in the early stages of cell development and is commonly found on cell surfaces and in matrix vesicles of bone and calcified cartilage (41). Although some osteocalcin genes are upregulated, ALP expression decreases (42). The expression of RUNX2 marks the onset of osteoblast differentiation and promotes the early maturation and differentiation of osteoblasts (43). Therefore, RUNX2 is the earliest and most specific marker of the bone formation process and is generally highly expressed in the early stage of bone cell differentiation (44). BSP, a critical marker protein, is highly expressed in the middle and late stages of osteoblast differentiation (44). The results of the present study suggested that ALP, BSP and RUNX2 expression increased considerably in HERS cultured with DPSC-EVs, suggesting that DPSC-EVs promote osteogenic differentiation in HERS cells at an early stage. The results in the present study are consistent with previous studies, which indicated that HERS could differentiate into cementum cells through EMT and secrete cementum to form periodontal tissue (8,9). However, in the present study the role and regulatory mechanism of DPSC-EVs in the promotion of osteogenic differentiation of HERS cells was also investigated.

The findings of the present study revealed that EVs are crucial regulators of EMT and are essential for bone development and regeneration. EVs play a dual role in the aforementioned processes, activating endothelial cells to accelerate their migration and proliferation and stimulating osteogenesis by regulating osteogenic growth factors (45). EVs promote vascular invasion and the recruitment of fragmented cartilage tissue to hypertrophic cartilage (46). Thus, the results of the present study indicated that EMT and osteogenesis

are linked and must be tightly coupled for the physiological function of bones.

Although EV treatment has shown promising outcomes, the exact underlying mechanism remains unclear. Several studies have reported that TGF-β1 regulates various functions in normal tissue homeostasis, such as cellular differentiation, apoptosis, cell cycle arrest and cellular migration (47-49). TGF-β1 binds to type I receptors and forms a heteromeric complex with type II receptors (50). This complex activates intracellular Smad transcription factors to mediate downstream signaling events, which facilitates the movement of the complex into the nucleus, where it regulates the expression of its target genes (50). The *in vitro* results of the present study showed that DPSC-EVs mediate HERS cell functions through the cell surface presentation of TGF-β1 to TGF-βR on target cells. Furthermore, with Smad2 and Smad3 phosphorylation, the phosphorylated intermediate is associated with a co-Smad in the cytoplasm, which migrates to the nucleus, where transcription is regulated through direct DNA binding by the Smad complex. Thereafter, the expression of Smad2/3 and p-Smad2/3 in HERS cells was determined, and p-Smad2/3 and MAPK/ERK expression increased significantly following DPSC-EV treatment, whereas inhibiting TGF-β1 expression in HERS cells decreased p-Smad expression. These findings suggested that the combination of TGF-β1 on the surface of HERS cells activates downstream signal transducers of TGF-β1, including Smad2/3. Furthermore, these findings suggested that DPSC-EVs modulate osteogenesis via TGF-β1/ERK signaling. Micro-CT examinations were performed to observe bone regeneration in each rat group after injecting DPSC-EVs, DPSC-EV-loaded hydrogels or DPSC-EV-loaded hydrogels with TGF-β1i. New bone grew concentrically in the DPSC-EV or DPSC-EV-loaded hydrogel groups, with greater bone mass and BV/TV. *In vivo*, the expression of osteogenesis-related proteins was determined, and the expression of BSP, ALP and RUNX2 increased significantly following treatment with DPSC-EVs or DPSC-EV-loaded hydrogels, indicating that DPSC-EVs or DPSC-EV-loaded hydrogels might promote osteogenesis after alveolar bone defects. The present study had several limitations, including that the role of cytokines in EVs was not verified, and *in vivo* new bone regeneration and BMD were not be detected via histological examinations.

To summarize, the findings of the present study revealed that DPSC-EVs promote EMT and osteogenesis. DPSC-EVs promote the proliferation and EMT of HERS cells. The cell viability and proliferation results indicated that DPSC-EVs provide suitable conditions for HERS cells. Additionally, DPSC-EVs affect osteogenic differentiation through the TGF-β1/ERK signaling pathway. The DPSC-EVs and the DPSC-EV-loaded hydrogels greatly promoted osteogenesis in alveolar bone defect model rats. These findings suggested that DPSC-EVs or DPSC-EV-loaded hydrogels regulate osteogenesis, which might be a key therapeutic target for alveolar bone defects (Fig. 6).

Acknowledgements

Not applicable.

Funding

This work was supported by grants from the Beijing Nova Program (grant no. 20220484231) and China Higher Education Innovation Fund (grant no. 2021JH039).

Availability of data and materials

The data generated in the present study may be requested from the corresponding author.

Authors' contributions

XH, XYC, KY and DLZ conceived and designed the study. XH and XC performed the experiments, collected and analyzed the data, produced the figures and wrote the manuscript. XC, YLX, ZLL, YL and CYG performed bioinformatics and statistical analysis. YYL and KY revised the manuscript. KY and DLZ confirm the authenticity of all the raw data. All authors read and approved the final version of the manuscript.

Ethics approval and consent to participate

The present study was approved by The Animal Welfare Ethics Committee of Beijing MDKN Biotechnology Co., LTD. (Beijing, China; approval no. MDKN-2022-052).

Patient consent for publication

Not applicable.

Competing interests

The authors declare that they have no competing interests.

References

1. Hollý D, Klein M, Mazreku M, Zamborský R, Polák Š, Danišovič Ľ and Csöbönyeiová M: Stem cells and their derivatives-implications for alveolar bone regeneration: A comprehensive review. Int J Mol Sci 22: 11746, 2021.
2. Pervizaj-Oruqaj L, Selvakumar B, Ferrero MR, Heiner M, Malainou C, Glaser RD, Wilhelm J, Bartkuhn M, Weiss A, Alexopoulos I, *et al*: Alveolar macrophage-expressed Plet1 is a driver of lung epithelial repair after viral pneumonia. Nat Commun 15: 87, 2024.
3. Lu X, Yu S, Chen G, Zheng W, Peng J, Huang X and Chen L: Insight into the roles of melatonin in bone tissue and bone-related diseases (Review). Int J Mol Med 47: 82, 2021.
4. Baldwin P, Li DJ, Auston DA, Mir HS, Yoon RS and Koval KJ: Autograft, allograft, and bone graft substitutes: Clinical evidence and indications for use in the setting of orthopaedic trauma surgery. J Orthop Trauma 33: 203-213, 2019.
5. Wang HD and Zhang YZ: Editorial commentary: Reduce the failure risk: A challenge to reduce the risk of using hybrid graft in anterior cruciate ligament reconstruction. Arthroscopy 34: 2936-2938, 2018.
6. Lei F, Li M, Lin T, Zhou H, Wang F and Su X: Treatment of inflammatory bone loss in periodontitis by stem cell-derived exosomes. Acta Biomater 141: 333-343, 2022.
7. Li X, Zhang S, Zhang Z, Guo W, Chen G and Tian W: Development of immortalized Hertwig's epithelial root sheath cell lines for cementum and dentin regeneration. Stem Cell Res Ther 10: 3, 2019.
8. Ouchi T and Nakagawa T: Mesenchymal stem cell-based tissue regeneration therapies for periodontitis. Regen Ther 14: 72-78, 2020.

9. Park KR, Kim S, Cho M and Yun HM: Limonoid triterpene, obacunone increases runt-related transcription factor 2 to promote osteoblast differentiation and function. Int J Mol Sci 22: 2483, 2021.
10. Bi F, Tang H, Zhang Z, Lyu Y, Huo F, Chen G and Guo W: Hertwig's epithelial root sheath cells show potential for periodontal complex regeneration. J Periodontol 94: 263-276, 2023.
11. Zhang S, Yang Y, Jia S, Chen H, Duan Y, Li X, Wang S, Wang T, Lyu Y, Chen G and Tian W: Exosome-like vesicles derived from Hertwig's epithelial root sheath cells promote the regeneration of dentin-pulp tissue. Theranostics 10: 5914-5931, 2020.
12. Gupta D, Zickler AM and El Andaloussi S: Dosing extracellular vesicles. Adv Drug Deliv Rev 178: 113961, 2021.
13. Harrell CR, Jovicic N, Djonov V, Arsenijevic N and Volarevic V: Mesenchymal stem cell-derived exosomes and other extracellular vesicles as new remedies in the therapy of inflammatory diseases. Cells 8: 1605, 2019.
14. Mattei V and Delle Monache S: Dental pulp stem cells (DPSCs) and tissue regeneration: Mechanisms mediated by direct, paracrine, or autocrine effects. Biomedicines 11: 386, 2023.
15. Mattei V, Martellucci S, Pulcini F, Santilli F, Sorice M and Delle Monache S: Regenerative potential of DPSCs and revascularization: direct, paracrine or autocrine effect? Stem Cell Rev Rep 17: 1635-1646, 2021.
16. Wang X and Thomsen P: Mesenchymal stem cell-derived small extracellular vesicles and bone regeneration. Basic Clin Pharmacol Toxicol 128: 18-36, 2021.
17. Zhang S, Chuah SJ, Lai RC, Hui JHP, Lim SK and Toh WS: MSC exosomes mediate cartilage repair by enhancing proliferation, attenuating apoptosis and modulating immune reactivity. Biomaterials 156: 16-27, 2018.
18. Hade MD, Suire CN and Suo Z. Mesenchymal stem cell-derived exosomes: applications in regenerative medicin. Cells 10: 1959, 2021.
19. Otsuru S, Desbourdes L, Guess AJ, Hofmann TJ, Relation T, Kaito T, Dominici M, Iwamoto M and Horwitz EM: Extracellular vesicles released from mesenchymal stromal cells stimulate bone growth in osteogenesis imperfecta. Cytotherapy 20: 62-73, 2018.
20. Familtseva A, Jeremic N and Tyagi SC: Exosomes: Cell-created drug delivery systems. Mol Cell Biochem 459: 1-6, 2019.
21. Wu F, Lei N, Yang S, Zhou J, Chen M, Chen C, Qiu L, Guo R, Li Y and Chang L: Treatment strategies for intrauterine adhesion: Focus on the exosomes and hydrogels. Front Bioeng Biotechnol 11: 1264006, 2023.
22. Chew JRJ, Chuah SJ, Teo KYW, Zhang S, Lai RC, Fu JH, Lim LP, Lim SK and Toh WS: Mesenchymal stem cell exosomes enhance periodontal ligament cell functions and promote periodontal regeneration. Acta Biomater 89: 252-264, 2019.
23. Kandalam U, Kawai T, Ravindran G, Brockman R, Romero J, Munro M, Ortiz J, Heidari A, Thomas R, Kuriakose S, *et al*: Predifferentiated gingival stem cell-induced bone regeneration in rat alveolar bone defect model. Tissue Eng Part A 27: 424-436, 2021.
24. Fang CH, Sun CK, Lin YW, Hung MC, Lin HY, Li CH, Lin IP, Chang HC, Sun JS and Chang JZ: Metformin-incorporated gelatin/nano-hydroxyapatite scaffolds promotes bone regeneration in critical size rat alveolar bone defect model. Int J Mol Sci 23: 558, 2022.
25. Guo Q, Zheng J, Lin H, Han Z, Wang Z, Ren J, Zhai J, Zhao H, Du R and Li C: Conditioned media of deer antler stem cells accelerate regeneration of alveolar bone defects in rats. Cell Prolif 56: e13454, 2023.
26. Witwer KW, Goberdhan DC, O'Driscoll L, Théry C, Welsh JA, Blenkiron C, Buzás EI, Di Vizio D, Erdbrügger U, Falcón-Pérez JM, *et al*: Updating MISEV: Evolving the minimal requirements for studies of extracellular vesicles. J Extracell Vesicles 10: e12182, 2021.
27. Gelibter S, Marostica G, Mandelli A, Siciliani S, Podini P, Finardi A and Furlan R: The impact of storage on extracellular vesicles: A systematic study. J Extracell Vesicles 11: e12162, 2022.
28. Matsuzaka Y and Yashiro R: Therapeutic strategy of mesenchymal-stem-cell-derived extracellular vesicles as regenerative medicine. Int J Mol Sci 23: 6480, 2022.
29. Storti G, Scioli MG, Kim BS, Orlandi A and Cervelli V: Adipose-derived stem cells in bone tissue engineering: Useful tools with new applications. Stem Cells Int 2019: 3673857, 2019.
30. Wan Z, Zhang P, Liu Y, Lv L and Zhou Y: Four-dimensional bioprinting: Current developments and applications in bone tissue engineering. Acta Biomater 101: 26-42, 2020.
31. Chen Y, Yang Q, Lv C, Chen Y, Zhao W, Li W, Chen H, Wang H, Sun W and Yuan H: NLRP3 regulates alveolar bone loss in ligature-induced periodontitis by promoting osteoclastic differentiation. Cell Prolif 54: e12973, 2021.
32. Lin W, Li Q, Zhang D, Zhang X, Qi X, Wang Q, Chen Y, Liu C, Li H, Zhang S, *et al*: Mapping the immune microenvironment for mandibular alveolar bone homeostasis at single-cell resolution. Bone Res 9: 17, 2021.
33. Kittaka M, Yoshimoto T, Schlosser C, Rottapel R, Kajiya M, Kurihara H, Reichenberger EJ and Ueki Y: Alveolar bone protection by targeting the SH3BP2-SYK axis in osteoclasts. J Bone Miner Res 35: 382-395, 2020.
34. Huang X, Xie M, Xie Y, Mei F, Lu X, Li X and Chen L: The roles of osteocytes in alveolar bone destruction in periodontitis. J Transl Med 18: 479, 2020.
35. Tan J, Dai A, Pan L, Zhang L, Wang Z, Ke T, Sun W, Wu Y, Ding PH and Chen L: Inflamm-aging-related cytokines of IL-17 and IFN-γ accelerate osteoclastogenesis and periodontal destruction. J Immunol Res 2021: 9919024, 2021.
36. Zhu L, Zhou C, Chen S, Huang D, Jiang Y, Lan Y, Zou S and Li Y: Osteoporosis and alveolar bone health in periodontitis niche: A predisposing factors-centered review. Cells 11: 3380, 2022.
37. Setiawan M, Jäger A, Daratsianos N, Reimann S, Chen J, Schmöle AC, Derichs-Schönthal D and Konermann A: Impact of the endocannabinoid system on murine cranial and alveolar bone phenotype. Ann Anat 230: 151516, 2020.
38. Martínez-Gil N, Mellibovsky L, Manzano-López González D, Patiño JD, Cozar M, Rabionet R, Grinberg D and Balcells S: On the association between Chiari malformation type 1, bone mineral density and bone related genes. Bone Rep 16: 101181, 2022.
39. Vimalraj S: Alkaline phosphatase: Structure, expression and its function in bone mineralization. Gene 754: 144855, 2020.
40. Cirano FR, Pimentel SP, Ribeiro FV, Casati MZ, Casarin RC, Gallafassi DF, Nishii D and Corrêa MG: Impact of history of periodontitis on gene expression of bone-related factors in young patients. Braz Oral Res 34: e014, 2020.
41. Balbaied T and Moore E: Overview of optical and electrochemical alkaline phosphatase (ALP) biosensors: Recent approaches in cells culture techniques. Biosensors (Basel) 9: 102, 2019.
42. Darjanki CM, Prahasanti C, Fitria AE, Kusumawardani B, Wijaksana IKE and Aljunaid M: RUNX2 and ALP expression in osteoblast cells exposed by PMMA-HAp combination: An in vitro study. J Oral Biol Craniofac Res 13: 277-282, 2023.
43. Kim KM, Son HE, Min HY and Jang WG: Vitexin enhances osteoblast differentiation through phosphorylation of Smad and expression of Runx2 at in vitro and ex vivo. Mol Biol Rep 47: 8809-8817, 2020.
44. Gao RT, Zhan LP, Meng C, Zhang N, Chang SM, Yao R and Li C: Homeobox B7 promotes the osteogenic differentiation potential of mesenchymal stem cells by activating RUNX2 and transcript of BSP. Int J Clin Exp Med 8: 10459-10470, 2015.
45. Chen D, Kim DJ, Shen J, Zou Z and O'Keefe RJ: Runx2 plays a central role in Osteoarthritis development. J Orthop Translat 23: 132-139, 2020.
46. Kazemi NY, Gendrot B, Berishvili E, Markovic SN and Cohen M: The role and clinical interest of extracellular vesicles in pregnancy and ovarian cancer. Biomedicines 9: 1257, 2021.
47. Gug C, Caba L, Mozos I, Stoian D, Atasie D, Gug M and Gorduza EV: Rare splicing mutation in COL1A1 gene identified by whole exomes sequencing in a patient with osteogenesis imperfecta type I followed by prenatal diagnosis: A case report and review of the literature. Gene 741: 144565, 2020.
48. Zhang L, Hu J, Meshkat BI, Liechty KW and Xu J: LncRNA MALAT1 modulates TGF-β1-induced EMT in keratinocyte. Int J Mol Sci 22: 11816, 2021.
49. Syed AM, Kundu S, Ram C, Kulhari U, Kumar A, Mugale MN, Mohapatra P, Murty US and Sahu BD: Up-regulation of Nrf2/HO-1 and inhibition of TGF-β1/Smad2/3 signaling axis by daphnetin alleviates transverse aortic constriction-induced cardiac remodeling in mice. Free Radic Biol Med 186: 17-30, 2022.
50. Wang J, Xiang H, Lu Y and Wu T: Role and clinical significance of TGF-β1 and TGF-βR1 in malignant tumors (Review). Int J Mol Med 47: 55, 2021.